

LJMU Research Online

Graef, F, Richtert, R, Fetz, V, Murgia, X, De Rossi, C, Schneider-Daum, N, Allegretta, G, Elgaher, W, Hauipenthal, J, Empting, M, Beckmann, F, BroEnstrup, M, Hartmann, R, Gordon, S and Lehr, C-M

In Vitro Model of the Gram-Negative Bacterial Cell Envelope for Investigation of Anti-Infective Permeation Kinetics

<http://researchonline.ljmu.ac.uk/id/eprint/10276/>

Article

Citation (please note it is advisable to refer to the publisher's version if you intend to cite from this work)

Graef, F, Richtert, R, Fetz, V, Murgia, X, De Rossi, C, Schneider-Daum, N, Allegretta, G, Elgaher, W, Hauipenthal, J, Empting, M, Beckmann, F, BroEnstrup, M, Hartmann, R, Gordon, S and Lehr, C-M (2018) In Vitro Model of the Gram-Negative Bacterial Cell Envelope for Investigation of Anti-

LJMU has developed **LJMU Research Online** for users to access the research output of the University more effectively. Copyright © and Moral Rights for the papers on this site are retained by the individual authors and/or other copyright owners. Users may download and/or print one copy of any article(s) in LJMU Research Online to facilitate their private study or for non-commercial research. You may not engage in further distribution of the material or use it for any profit-making activities or any commercial gain.

The version presented here may differ from the published version or from the version of the record. Please see the repository URL above for details on accessing the published version and note that access may require a subscription.

For more information please contact researchonline@ljmu.ac.uk

<http://researchonline.ljmu.ac.uk/>

An *In Vitro* Model of the Gram-Negative Bacterial Cell Envelope for Investigation of Anti-Infective Permeation Kinetics

Florian Graef^{1,2*}, Robert Richter^{1,2*}, Verena Fetz^{3,4}, Xabier Murgia^{1,2}, Chiara De Rossi¹, Nicole Schneider-Daum¹, Giuseppe Allegretta⁵, Walid Elgaher⁵, Jörg Hauptenthal⁵, Martin Empting^{2,5}, Felix Beckmann⁶, Mark Brönstrup³, Rolf Hartmann^{2,5}, Sarah Gordon^{1,7#} and Claus-Michael Lehr^{1, 2#}

¹ Department Drug Delivery, Helmholtz Institute for Pharmaceutical Research Saarland (HIPS), Helmholtz Center for Infection Research (HZI), Saarland University Campus, Building E8 1; 66123 Saarbrücken, Germany

² Department of Pharmacy, Saarland University, University Campus, Building E8 1, 66123 Saarbrücken, Germany

³ Department Chemical Biology, HZI, German Center for Infection Research, Inhoffenstraße 7, 38124 Braunschweig, Germany

⁴ School of Engineering and Science, Jacobs University Bremen, Campus Ring 1, 28759 Bremen, Germany

⁵ Department Drug Design and Optimization, HIPS, HZI, Saarland University Campus, Building E8 1; 66123 Saarbrücken, Germany

⁶ Institute of Materials Research, Helmholtz-Zentrum Geesthacht, Max-Planck-Straße 1, 21502 Geesthacht, Germany

⁷ School of Pharmacy and Biomolecular Sciences, Liverpool John Moores University, James Parsons Building, Byrom Street, L3 3AF Liverpool, United Kingdom

* equally contributing

Corresponding Authors:

S.C.Gordon@ljmu.ac.uk; Claus-michael.lehr@helmholtz-hzi.de

The cell envelope of Gram-negative bacteria is a formidable biological barrier, inhibiting the action of antibiotics by impeding their permeation into the intracellular environment. In-depth understanding of permeation through this barrier remains a challenge, despite its critical role in antibiotic activity. We therefore designed a divisible *in vitro* permeation model of the Gram-negative bacterial cell envelope, mimicking its three essential structural elements – the inner membrane, the periplasmic space as well as the outer membrane – on a Transwell® setup. The model was characterized by contemporary imaging techniques and employed to generate reproducible quantitative and time-resolved permeation data for various fluorescent probes and anti-infective molecules of different structure and physicochemical properties. For a set of three fluorescent probes the permeation through the overall membrane model was found to correlate with *in bacterio* permeation. Even more interestingly, for a set of six *Pseudomonas* quorum sensing inhibitors, such permeability data were found to be predictive for their corresponding *in bacterio* activities. Further exploration of the capabilities of the overall model yielded a correlation between the permeability of porin-

independent antibiotics and published *in bacterio* accumulation data; a promising ability to provide structure-permeability information was also demonstrated. Such a model may therefore constitute a valuable tool for the development of novel anti-infective drugs.

Keywords: Anti-infectives, drug delivery, drug design, Gram-negative bacterial cell envelope, *in vitro* model

Infectious diseases caused by Gram-negative bacteria are becoming increasingly difficult to treat, due to the significant and evolving protective effect of the bacterial cell envelope.¹ A comprehensive analysis has demonstrated that the major scientific obstacle to the discovery of novel, Gram-negative active antibiotics is an insufficient understanding of how to design molecules capable of overcoming this barrier.^{2, 3} The envelope itself consists of a largely phospholipid-based inner membrane (IM), a peptidoglycan-containing periplasmic space (PS), and an asymmetric outer membrane (OM) composed of a phospholipid-containing inner leaflet (IL) and a lipopolysaccharide (LPS)-based outer leaflet (OL).⁴ Clearly therefore, the Gram-negative cell envelope constitutes a complex and considerable physical barrier to the entry and subsequent action of anti-infectives.⁵

Given that trafficking of anti-infectives into and across the envelope barrier is an essential requirement for their activity, the ability to assess anti-infective permeation in a quantitative, kinetically-resolved manner would offer considerable advantages.⁶ High content permeation information and the afforded ability to establish structure-permeability relationships would represent valuable tools in the rational design and

optimization of anti-infectives⁷. This would additionally complement the assessment of drug-target interactions as well as classical efficacy testing such as the determination of minimum inhibitory concentrations (MIC).⁸ The use of bacterial cell assays, as the most representative means for assessing envelope permeation kinetics, is possible, but is hampered by considerable analytical and practical challenges.⁹ A wealth of *in vitro* envelope models is also available, generally grouped into the categories of Langmuir film-based models,¹⁰ electrophysiology models,^{11, 12} and vesicle-based assays.¹³ However, many of these existing models do not entirely approximate the double membrane structure of the cell envelope, or are composed of phospholipids which differ in either species or quantity from those found in Gram-negative bacteria. As a result, the majority of these existing models are not sufficiently representative of the overall envelope structure to allow for determination of envelope permeation kinetics, and additionally lack the level of robustness required for such investigations.^{12,}
¹⁴ A clear need therefore exists for *in vitro* models that are specifically designed and suited for the assessment of bacterial envelope permeation. Although transport processes in bacteria are mediated to a significant extent by transmembrane proteins, a method to assess passive diffusion processes across the envelope membranes was nevertheless hypothesized to be valuable, as it would allow for identification of compounds whose entry is (at least in part) protein-independent, or may become so due to saturation or downregulation. The ability to characterize passive envelope permeation independent of active protein-mediated transport could potentially also aid in the differentiation of compounds which are simply poorly permeable, from compounds which have an appreciable membrane permeability but do not appear to reach or be retained at their target site due to active efflux.

Having previously demonstrated the potential of such a setup by developing a model that assesses passive permeation across the bacterial IM alone,¹⁵ we herein report on the design of a divisible *in vitro* permeation model of the entire Gram-negative cell envelope. The model consists of IM and OM structures separated by a gel-based spacer as a surrogate for the PS. It was prepared stepwise by generating individual OM and PS structures, which were then combined with the previously developed IM model (Figure 1). Individual structures as well as the overall envelope model itself were fabricated by deposition on culture plate filter inserts of the Transwell® system – the membrane filter of which is commonly used to support mammalian cell monolayers employed in permeation studies.¹⁶ While entailing significant dimensional scale up (for instance in thickness) in comparison to native bacteria, the employment of a Transwell®-based modeling approach provides a solution to the aforementioned issues of robustness, resolution and quantification associated with existing cell-based and *in vitro* bacterial models.

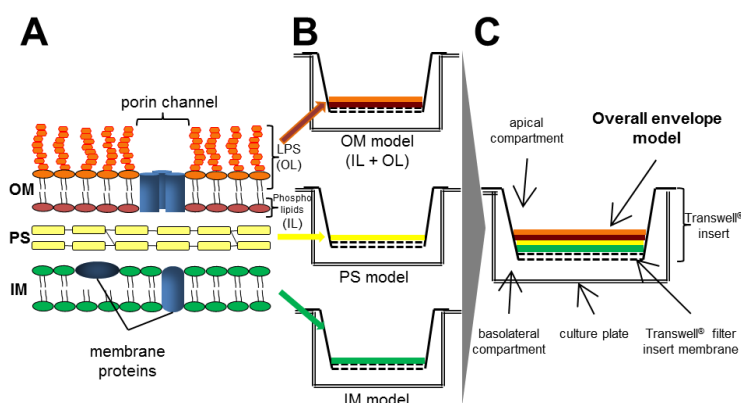


Figure 1. Schematic of the Gram-negative bacterial cell envelope and modeling approach. The envelope consists of the inner membrane (IM), the periplasmic space (PS) and the outer membrane (OM), with its phospholipid-containing inner leaflet (IL) and lipopolysaccharide (LPS)-containing outer leaflet (OL) (A). The individual modeling approach of each envelope component is shown (B); in addition, the overall envelope

model setup is depicted (C). In all cases, the antibiotic permeability can be assessed by addition of the drug to the apical compartment, followed by a quantification of drug concentration of basolateral compartment samples over time.

Results and Discussion

In the development of an OM model, it was aimed to mimic the asymmetric nature of IL and OL structures in order to obtain a functional similarity to the native OM. The modeling procedure consisted of two coating processes. First, Transwell® inserts were coated with a physiologically relevant 90:10 weight ratio of palmitoyl-oleoyl-phosphatidylethanolamine (POPE) and palmitoyl-oleoyl-phosphatidylglycerol (POPG), as a composition representative of *Escherichia coli*,¹⁷ in order to form the IL (Figure 2A 1). In a second step, LPS was deposited on top of the IL via a customized nebulization chamber, to form the OL component of the OM (Figure 2A 2). The OM model was characterized in terms of structure and suitability for transport experiments, prior to assessment of its functional similarity to the bacterial OM. An increase in z-dimension when comparing the IL+OL containing OM model with the IL structure alone was taken as a first indication of the successful deposition of an LPS layer (Figure S1).

The integrity of the LPS-based OL (known to be chiefly responsible for OM barrier properties¹⁸) was confirmed via confocal laser scanning microscopy (CLSM) and found to be robust and stable for several hours under conditions of transport experiments (Figure S2). Correlative microscopy allowed for visualization of a sufficient coverage and distribution of LPS deposited on top of the phospholipids of the IL (Figure 2B-D).

Complementarily, the asymmetric structure of the entire OM could be clearly shown via CLSM (Figure 3 A-C).

Transport studies with fluorescein, rhodamine 123 and rhodamine B isothiocyanate as permeability markers with varying lipophilicities (Table S1) confirmed the importance of combining IL and OL structures for achieving a functional OM surrogate, as significantly lower marker permeability was observed compared to experiments with the OL or IL alone (Figure S3). In order to investigate the specific functional similarity of the OM model to the native OM, the permeation of the aforementioned markers was measured in the presence of polymyxin B (PMB), a peptide known to permeabilize the native bacterial OM.¹⁹ An increased permeation was indeed observed for all three fluorescent dyes (Figure 3D). In a second step, the permeation of vancomycin, known to be inactive against Gram-negative bacteria due to its inability to cross the bacterial OM, was assessed.²⁰ Permeation of vancomycin was found to be very low (< 0.3% after 2.5 h, in comparison to values of 2-8% for the fluorescent compounds - Figure S3), confirming a functional similarity of the OM model to the native OM.

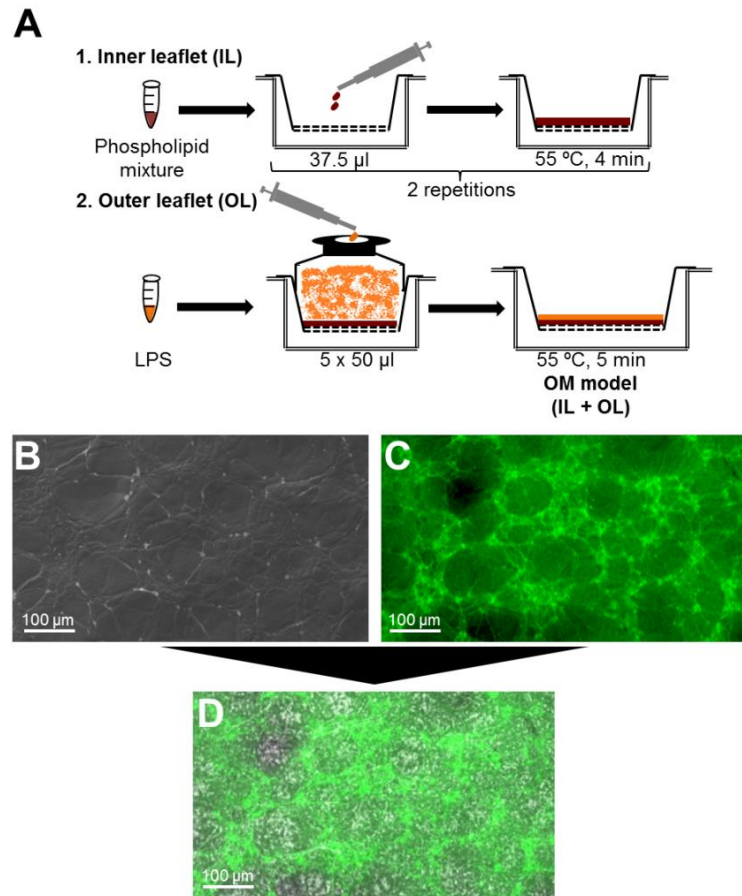


Figure 2. Outer membrane model preparation and characterization. Schematic of the two-step preparation process of the OM model (A). Representative scanning electron microscopy (SEM, B) and CLSM images (C) of the OM, showing fluorescently-labeled LPS in green. The superimposed correlative microscopy image (D) shows a sufficient coverage of the phospholipid layer with LPS (in accordance with Figure S2) as well as some spot-wise accumulation, potentially as a result of the IL surface texture.

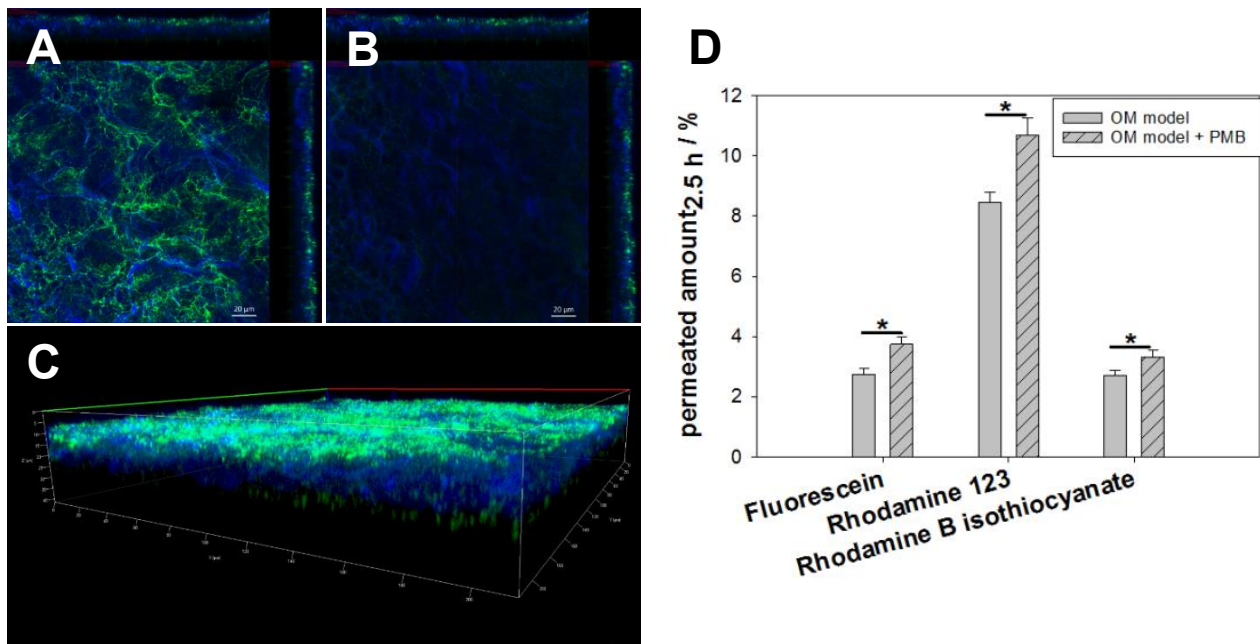


Figure 3. CLSM imaging and functional assessment of the OM. Using CLSM the orthographic projection of the OM model shows fluorescein isothiocyanate (FITC)-labeled LPS of the OL in green and laurdan stained PLs of the IL in blue (A). Orthographic projection of the same sample, but on a lower level in z-direction, shows the separation of LPS of the OL from PL of the IL (B). This demonstrates the asymmetric structure of the OM model, which is also evident from the three-dimensional view (C). The permeabilizing effect of PMB on the OM model is shown by the increased translocation of the three dyes (D), confirming functional similarity to the native OM. Values represent mean \pm SE; $n=9$ from three independent experiments.

Next, a PS model was prepared. The PS is not considered to constitute a diffusion barrier in the order of the IM and OM,²¹ but rather serves as a hydrophilic, viscous spacer compartment separating the two lipophilic membrane structures.⁴ An alginate gel layer was employed for this purpose. The suitability of this layer was tested in permeation studies using the two fluorescent probes fluorescein and rhodamine B isothiocyanate, which show different lipophilicities and charges at the experimental pH

of 7.4. Comparing their permeation through the gel to uncoated Transwell® inserts, as well as to OM and IM models, showed that although the permeation through the alginate gel is slightly lower compared to the blank Transwell® insert, its impact is still negligible compared to the significantly lower permeability across OM and IM model structures. The observed absence of a pronounced diffusion barrier property of the PS model compared to the IM and OM model hence demonstrates functional similarity of the PS model to the native PS.

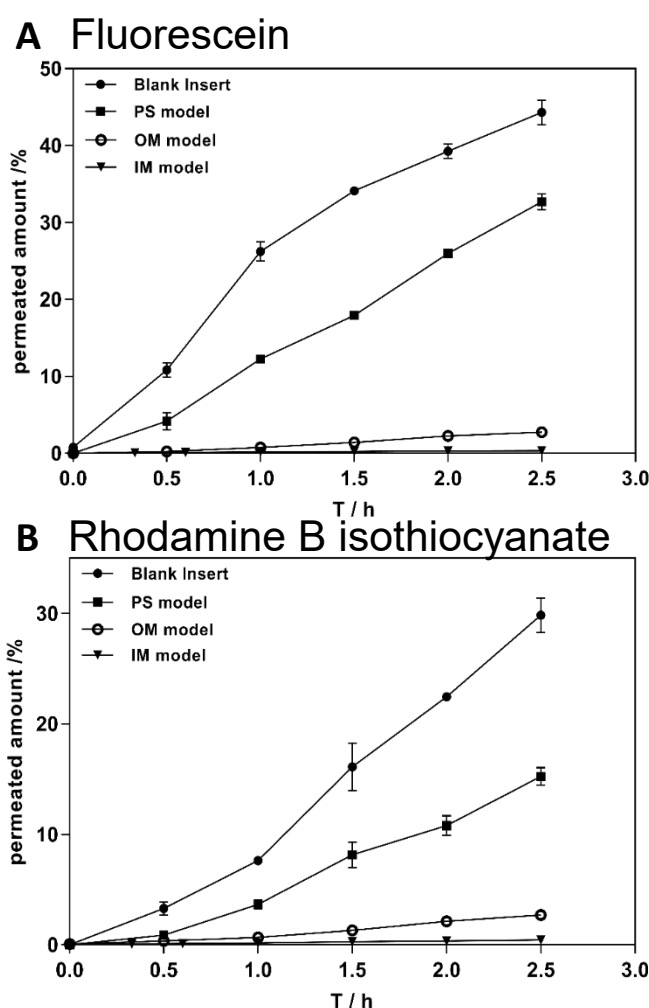


Figure 4. Permeated amounts of fluorescein (A) and rhodamine B isothiocyanate (B) across the PS model in comparison to an uncoated Transwell® membrane, the OM model and the IM model. Values represent mean \pm SE; n=3 for PS model and blank

insert experiments; n=9 from 3 individual experiments for IM and OM model experiments.

To obtain a model of the overall Gram-negative bacterial cell envelope, the previously developed IM was first deposited on a Transwell® insert; this was then overlaid with the gel of the PS, on top of which the OM was deposited. As demonstrated by SEM, the alginate layer utilized as the PS serves as a robust spacer between the IM and OM, without being affected by application of the OM (Figure S4). The three-layered structure of the entire envelope model was demonstrated by CLSM (Figure S5).

Clearly, the value of such an *in vitro* model as a tool for optimizing anti-infective compounds strongly depends on the predictivity of obtained permeation data. In a first step towards gauging this value, we compared permeation data of fluorescent permeability markers in our *in vitro* model with cellular uptake data, obtained by quantifying compound translocation in *E. coli* by liquid chromatography-tandem mass spectrometry (LC-MS/MS). For this purpose, fluorescein, rhodamine 123 and rhodamine B were selected due to their different $\log D_{\text{pH}7.4}$ values and varying charges at pH 7.4 (Table S1). The initial employment of non-antibiotic permeability markers further allowed for specific assessment of bacterial uptake without the confounding effect of bacterial killing. An increase of permeation/uptake as a function of permeability marker lipophilicity was observed in both the *in vitro* envelope model after 4.5 h of permeation studies, and in the *E. coli* cellular model; furthermore, the degree of marker uptake *in bacterio* showed similar levels to the percentage of compound permeation across the *in vitro* model (Figure 5A). In contrast to these rather cumbersome bacterial uptake studies, which may only provide a single data point due to their destructive nature, the new *in vitro* model allows for ready generation of time-resolved kinetic data of such permeation processes (Figure 5B).

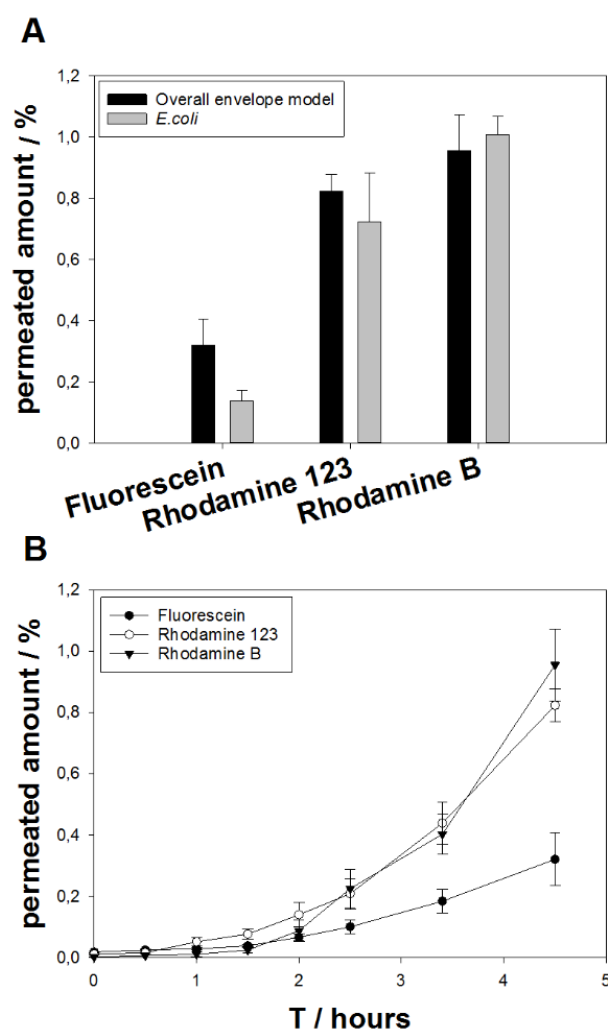
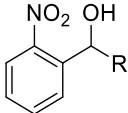


Figure 5. Comparison of permeability of marker compounds across the *in vitro* envelope model with uptake into *E. coli*. Permeability experiment results reveal comparable levels of uptake/permeation (A), while kinetic profiles of marker permeation highlight the ability of the *in vitro* envelope model to provide time-resolved permeation data (B). Values represent mean \pm SE; n=6 from two independent experiments.

In a second step, we selected a set of in-house synthesized quorum sensing inhibitors for permeation testing (Table 1, Figure S6). This new class of anti-infectives interferes with bacterial cell-to-cell communication and virulence by inhibiting the key signal molecule synthase PqsD of the human pathogen *Pseudomonas aeruginosa*.²² This

results in a reduced production of quorum sensing signals and related effector molecules.^{23, 24} PqsD inhibitors constitute an interesting group of compounds for testing in the overall envelope model, as they must permeate across the entire bacterial cell envelope in order to reach their intracellular target and do not affect bacterial growth. The selected compounds are of particular interest, as they exhibit comparable IC₅₀ values at their molecular target *in vitro*, but in some cases (compounds **1** and **2**) no *in bacterio* activity, represented by an absence of HHQ inhibition (Table 1).²⁵

Table 1. Important physicochemical parameters and activity in cell-free and cellular assays of PqsD inhibitors.

Compound	M _w	logP ^a	IC ₅₀	HHQ	% permeated ^{2.5h}
	(g/mol)		(μM) ^a	inhibition (%) ^{a,b}	(overall envelope model) ^c
1 , R = n-pentyl	223.27	3.24	1.0	no inhibition	Not detectable
2 , R = n-butyl	209.24	2.72	2.9	no inhibition	2.3 ± 0.2
3 , R = n-propyl	195.22	2.17	1.0	22	4.7 ± 0.4
4 , R = ethyl	181.19	1.64	0.8	61	8.9 ± 0.9
5 , R = methyl	167.16	1.11	0.8	26	9.2 ± 0.4
6 , R = H	153.14	0.76	0.7	13	12.8 ± 0.7

[a] Values from Storz *et al.*²⁵ [b] Readout for compound efficacy, determined in *P. aeruginosa* PA14 pqsH mutant at inhibitor concentrations of 250 μM. No inhibition was defined as <10 %. [c] Values represent mean ± SE, n=6 from 2 individual experiments.

The permeation behavior of compounds **1-6** was therefore tested in the overall envelope model, as a possible means of explaining observed differences in efficacy in spite of comparable target-based activity. Consistent with our hypothesis, PqsD inhibitors with HHQ inhibition and thus activity against *P. aeruginosa* (compounds **3**, **4**, **5**, and **6**) showed a significantly higher permeability across the envelope model in comparison to the non-active compounds (**1** and **2**; Table 1; Figure 6A, B). The permeability of compound **1** was even below the limit of assay detection. Interestingly, in direct contrast to the permeation behavior of fluorescent permeability markers (Figure 5A), PqsD inhibitor lipophilicity tended to be inversely correlated with cell envelope permeability. This observation implies an impact of physicochemical parameters additional to lipophilicity on compound permeation. Of further interest was the lack of a clear correlation between greatest activity against *P. aeruginosa* and highest *in vitro* permeability – this valuable observation may indicate a contribution of active efflux systems. Clustering of PqsD inhibitors based on their activity against *P. aeruginosa* and model permeability (Figure 6C) does however allow for a clear differentiation of the investigated PqsD inhibitors into two groups – compounds with a low model permeability ~ no *in bacterio* activity, and compounds with high model permeability ~ *in bacterio* activity. This data demonstrates the importance of cell envelope permeability as a delimiter of intracellular activity, and points to the usefulness of such data for the optimization of novel anti-infective compounds.

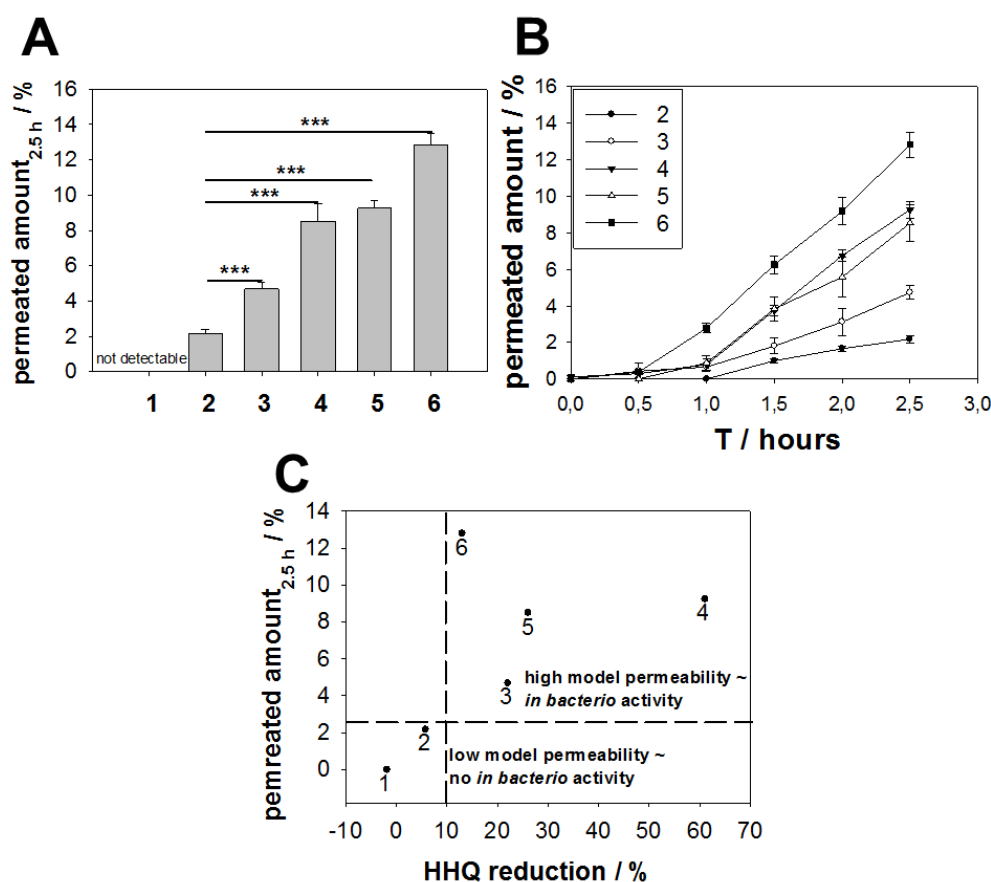


Figure 6. Permeability investigations of PqsD inhibitors. Permeability of the compounds **1-6** across the *in vitro* envelope model showing significantly higher permeation values in the case of *in bacterio*-active compounds in comparison to non-active ones (A). The depicted kinetic profiles highlight the ability of the overall envelope model setup to provide quantitative and kinetically-resolved permeation data (B). Compounds were furthermore clustered into two groups according to their permeation and their *in bacterio* activity (% HHQ reduction at a compound concentration of 250 μ M) (C). Values represent mean \pm SE; n=6 from two individual experiments, *** = $P < 0.001$.

Further to the above findings, specific mention must be made of the fact that not all anti-infectives exhibit an activity which can be directly correlated to their membrane permeability. The influence of additional factors such as the intrinsic *in vitro* activity of anti-infectives, as well as their status as substrates of active efflux pumps, which are

not featured in the overall model in its current stage of development, must be also considered when evaluating anti-infective efficacy. This was demonstrated by additional permeability investigations utilizing a set of in house-synthesized RNA polymerase (RNAP) inhibitors (Table S4, Figure S6).

At this stage, as it had been noted that the structure of the overall membrane model still appeared to feature a rather uneven surface (Figure 7A), the protocol for PS preparation was improved by nebulizing rather than pipetting the component calcium chloride solution onto filter inserts. This resulted in a more planar overall membrane structure (Figure 7B).

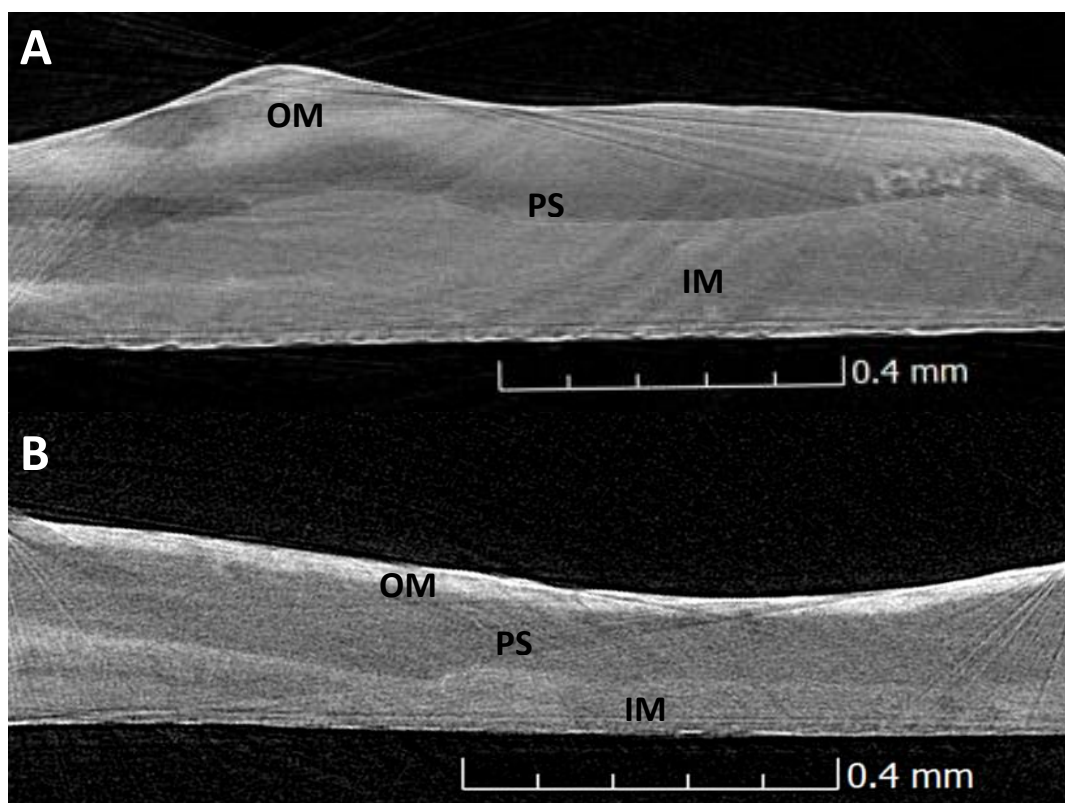


Figure 7. X-ray microtomographic images of the overall membrane model after the calcium chloride solution was pipetted (A) and after the calcium chloride solution was nebulized on top of the alginate gel (B). Nebulization according to the new protocol, thus led to a better separation of the three layers as well as the formation of a more even membrane structure.

After this modification, the capabilities of the model were further explored by assessing the permeability of a number of established antibiotics. In this respect, the permeation of novobiocin, erythromycin and rifampicin – reported to be passively permeating, porin-independent substances^{26,27} – was investigated. The permeation of the established antibiotic tetracycline, known for its largely porin-dependent permeation,²⁷⁻³⁰ was also determined. As depicted in Figure 8, novobiocin showed the lowest permeability of the porin-independent compounds, while erythromycin A (being the most abundant component of erythromycin) and rifampicin showed a higher and similar permeability. This is in nice agreement with a recently published study investigating

the accumulation of these compounds in porin-competent *E. coli*.⁷ The comparatively low degree of tetracycline permeation observed in the overall envelope model is also entirely in line with its documented reliance on porins in order to permeate across the Gram-negative cell envelope, and is additionally validated by a high degree of observed accumulation in porin-competent *E. coli*.⁷

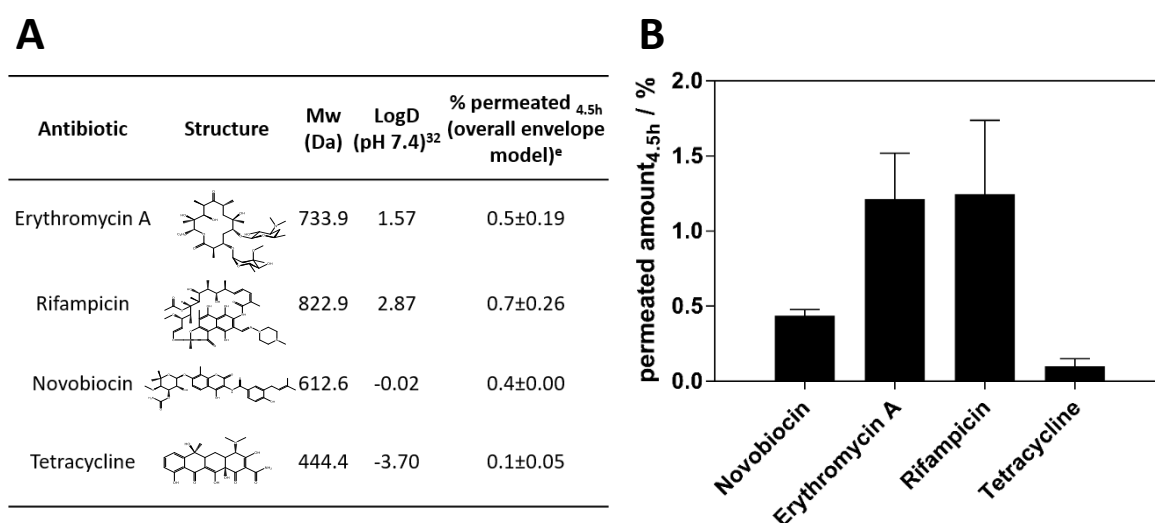


Figure 8. Permeability of the porin-independent antibiotics novobiocin, erythromycin A and rifampicin as well as the porin-dependent compound tetracycline across the improved overall envelope model. Compound characteristics can be seen in (A), with compound permeability shown in (B). [e] values represent mean \pm SE. $n \geq 10$ from three individual experiments.

Further steps towards the employment of the model for establishing structure-permeability relationships were then taken, by probing the permeability of the structurally-related gyrase inhibitors ciprofloxacin, norfloxacin, pipemidic acid and nalidixic acid (Figure 9). Nalidixic acid showed by far the highest degree of permeation of the tested compounds, likely due to its status as the smallest molecule of the tested set. The observed permeabilities of ciprofloxacin, norfloxacin, pipemidic acid and nalidixic acid were observed to increase with decreasing molecular weight (Mw),

indicating a stronger influence of this parameter than of compound polarity (LogD, Figure 9A). It is furthermore noteworthy, that the permeability of nalidixic acid was considerably higher than for the other gyrase inhibitors. This may be explained by the fact that, in contrast to nalidixic acid, the most abundant species of the comparatively lower permeating compounds ciprofloxacin, norfloxacin and pipemidic acid at pH 7.4 is the zwitterionic one.^{31,32} This corroborates the earlier reported inferior permeation of zwitterionic ciprofloxacin through a lipid layer compared to its neutral species.³³ This permeation behavior through porin-free membranes is, however, in contrast to porin-expressing *E. coli*, where a positive charge in particular seems to be necessary to allow for an enhanced access to the constriction region of the porins OmpF and OmpC.^{12, 34-37} Although at this stage still lacking specific transporters, such as porins and efflux pumps, the data obtained with the present model illustrate the value of such an approach to exclude e.g. poorly permeable candidates at a rather early stage of drug development, or to further optimize the design of novel anti-infectives towards better permeability.

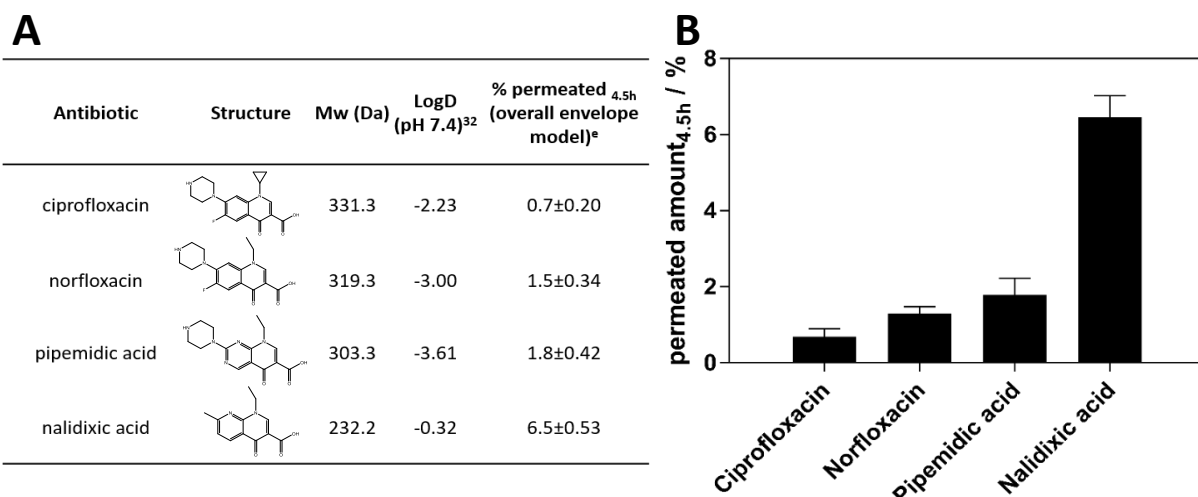


Figure 9. Permeation of structurally-related gyrase inhibitors in the improved overall envelope model. Compound structures and key physicochemical parameters are provided in (A), while compound permeability is shown in (B). [e] values represent mean \pm SE. $n \geq 11$ from three individual experiments.

In conclusion, we have realized a divisible *in vitro* model of the Gram-negative bacterial cell envelope, which allows for the collection of quantitative, time-resolved permeation data for anti-infective compounds. In the case of a set of innovative PqsD-inhibitors as well as a sample of established porin-independent antibiotics, overall envelope model permeability data could correctly predict *in bacterio* activity and bacterial accumulation respectively. Moreover, investigation of the permeability of a set of gyrase inhibitors showed a promising ability of the model to provide structure-permeability information. Further model development and optimization is currently ongoing in order to increase throughput capacity, to investigate quantitative structure permeability relationships and to incorporate porins as well as elements of active influx/efflux.

Methods

A detailed presentation of all utilized materials, preparation and characterization procedures can be found in the Supporting Information.

OM model preparation. Model preparation was optimized to obtain a structural mimic of the OM consisting of a phospholipid-containing IL overlaid by an LPS-containing OL. To form the IL, Transwell® filter inserts were coated in two cycles with 37.5 µL of a phospholipid mixture of POPE and POPG in a physiologically relevant 90:10 (weight) ratio,^{17, 38} with a drying step of 4 min at 55 °C using an incubator (Mettler UN75, Mettler GmbH & Co, KG; Schwabach, Germany) following each cycle. To prepare the OL, a 0.3 mg/mL LPS solution was then nebulized in five cycles onto the prepared IL structure, using an Aerogen Solo nebulizer (Aerogen Ltd, Galway, Ireland) together with an in-house developed nebulization chamber (see Supporting Information). A final drying step of 5 min at 55 °C was then employed.

OM model structural characterization. Correlative microscopy was performed to evaluate the integrity of LPS coverage in OM models. Filter inserts supporting OM structures were cut out of plastic holder surrounds, and sputter coated with gold (Quorum Q150R ES, Quorum Technologies Ltd., East Grinstead, UK). The Shuttle & Find™ extension and specialized sample holder (Carl Zeiss Microscopy GmbH, Germany) were used to image samples using both CLSM (Zeiss LSM 710, Jena, Germany) and SEM (Zeiss EVO HD 15, Carl Zeiss AG, Oberkochen, Germany), without the need for further sample alteration when switching between imaging methods. Further detail may be found in the Supporting Information.

CLSM was also used to further probe the OM structure, and in particular to confirm its asymmetric nature. The OM model was prepared as described above, employing

FITC-labeled LPS to form the outer leaflet (OL) and staining the IL with laurdan (ratio phospholipids to laurdan 400:1 mol/mol). Samples were subsequently cut out of the plastic holder support, attached to a glass slide using an adhesive fixing agent, and covered with a cover slip. Imaging was performed using a Zeiss LSM 710 Axio Observer (Carl Zeiss Microscopy GmbH, Jena, Germany; λ_{exc} = 405 nm and λ_{em} = 457 nm in the case of laurdan and λ_{exc} = 488 nm and λ_{em} = 564 nm in the case of FITC-labeled LPS).

OM model functional characterization. Transport studies were performed to investigate compound permeability through the OM. OM model-permeated amounts of fluorescent dyes (fluorescein sodium, rhodamine 123, and rhodamine B isothiocyanate, Table S1) were initially tested over an experimental period of 2.5 h (see Supporting Information for experimental details). OM transport studies employing PMB as a well-known bacterial OM permeabilizing agent were also conducted, to investigate the functional similarity of the OM model to the native bacterial OM. In this case, following equilibration in buffer, OM models were incubated for one hour with 500 μ L of 1.53 mM PMB. Following removal of PMB solutions and washing, fluorescent dyes were added and their permeability assessed as described in the Supporting Information.

PS model preparation. In what is referred to as the ‘standard protocol’, a 75 μ L volume of a 2% (w/v) alginate solution was added onto Transwell® filter inserts followed by the addition of 25 μ L of a 5% (w/v) calcium chloride solution. Filter inserts were then allowed to rest for at least 1 h at room temperature in order for gel formation to occur. An alteration to this protocol was later made (‘improved protocol’) in which five cycles of 100 μ L of a 5% (w/v) calcium chloride solution was nebulized per

Transwell®. The 20x increased volume relative to that employed above was chosen to compensate for the deposition efficiency of ~5% of the nebulization chamber.

PS model structural characterization. Transport studies using the PS model (standard preparation procedure) were carried out in order to confirm that this component did not constitute an appreciable barrier to compound permeation. Fluorescein and rhodamine B isothiocyanate were employed for this purpose as permeability markers with differing physical properties (Table S2). Transport experiments investigating the permeability behavior of both fluorescent dyes across blank Transwell® filter inserts as well as the PS model were performed as described above for the OM model (see above, as well as in the Supporting Information).

Overall envelope model preparation. The IM model was prepared as previously described.¹⁵ The PS model was then prepared directly on top of the IM structure, as described above. The IL and OL components of the OM were subsequently prepared on top of the PS, resulting in an overall envelope model.

Overall envelope model structural characterization. The structure of the overall envelope was characterized by X-ray microtomography employing beamline P05 operated by HZG at the storage ring PETRA III of DESY, Hamburg. Therefore, the overall membrane was prepared using the standard and the improved protocol (see above) for the PS and subsequently fixed and stained by exposing the coated Transwells® for 2 h to a 1% (w/v) OsO₄ solution. Afterwards, slices of 3 mm width and 12 mm length were cut out and placed into a thin plastic tube of 3 mm in diameter. Samples were exposed to X-ray synchrotron radiation using a photon energy of 12 keV. The tomographic reconstructions were performed from 1200 projections equally stepped while turning 180°. Visual data were processed employing VGSTUDIO MAX software, Volume Graphics GmbH, Heidelberg.

Overall envelope model functional characterization. The general procedure for permeability investigations in the OM model was also employed in the case of the overall envelope model. The permeation behavior of fluorescent dyes (fluorescein, rhodamine 123 and rhodamine B; Table S1), as well as that of in-house synthesized PqsD inhibitors (compounds 1, 2, 3, 4, 5 and 6, at a concentration of 400 μ M in buffer with 2% DMSO) was investigated. Moreover, the permeation of two sets of clinically established antibiotics – novobiocin, rifampicin and erythromycin as porin-independent antibiotics and tetracycline as a porin-dependent control, and the gyrase inhibitors ciprofloxacin, norfloxacin, pipemidic acid and nalidixic acid – was determined. Details of transport study methodology and quantification of compound permeation can be found in the Supporting Information.

In bacterio comparison – bacterial uptake studies. Intact *E. coli* (BW25113) cells, cultured as described in the Supporting Information, were incubated with 1 μ M solutions of fluorescein, rhodamine 123 or rhodamine B for 30 min. Cell suspension samples were then centrifuged through a 1 M sucrose cushion to remove adherent dye; resulting cell pellets were then sonicated with a probe sonicator (Sonoplus mini 20, Bandelin electronic GmbH Co. KG, Berlin, Germany) on ice in order to disrupt the bacterial cells. Following further centrifugation and extraction, internalized fluorescent dyes were quantified by LC-MS/MS, as detailed in the Supporting Information.

Statistical Analysis. Where appropriate, presented numerical data represent mean \pm standard error of the mean (SE). Student's t-test was employed where relevant to evaluate significant differences (**= $P < 0.01$, ***= $P < 0.001$). All tests were calculated using the software SigmaPlot version 12.5 (Systat Software, Inc., San Jose, California, USA).

Chemical structures. Structural formulae were created using ChemDraw® Professional Version 15.1.0.144 (PerkinElmer Informatics Inc., Waltham, MA, USA).

Supporting Information

Supporting Information Available: [Nebulization chamber characterization, OM model characterization, OM model transport experiments, robustness assessment of the PS model, structural assessment of the overall envelope model, overall envelope model transport experiments (RNAP inhibitors).] This material is available free of charge via the Internet at <http://pubs.acs.org>.

Abbreviations

CLSM, confocal laser scanning microscopy; FITC, fluorescein isothiocyanate; IL, inner leaflet; IM, inner membrane; LC-MS/MS, liquid chromatography-tandem mass spectrometry; LPS, lipopolysaccharide; MIC, minimum inhibitory concentration; OL, outer leaflet; OM, outer membrane; PMB, polymyxin B; POPG, palmitoyl-oleoyl-phosphatidylglycerol; POPE, palmitoyl-oleoyl-phosphatidylethanolamine; PS, periplasmic space; RNAP, RNA polymerase; SEM, scanning electron microscopy.

Author Information

Author Contribution

F. Graef led the model development studies (PS model, OM model and overall envelope model), performed model characterization (of the PS, OM model and overall

envelope model), permeability investigations (fluorescent dyes, PqsD and RNAP inhibitors), and equally contributed to writing the original manuscript draft.

R. Richter optimized the membrane model, performed permeability investigations, CLSM investigation of the outer membrane structure, X-ray microtomography and stereomicroscopic investigation of the overall membrane model, and equally contributed to writing the original manuscript draft.

V. Fetz performed the bacterial uptake studies.

X. Murgia equally contributed to the design of the nebulization chamber.

C. De Rossi performed CLSM investigations and LC-MS/MS quantification.

F. Beckmann performed X-ray microtomography of the overall membrane model.

G. Allegretta and W. Elgaher synthesized the RNAP and PqsD inhibitor compounds.

J. Haupenthal, M. Empting and R. Hartmann analyzed data, edited the manuscript and supported in project administration.

M.Brönstrup conceived studies, analyzed data and edited the manuscript.

S. Gordon, N. Schneider-Daum and C.-M. Lehr were responsible for project administration and writing of the original manuscript draft.

Conflict of Interest

The authors declare no competing financial interest.

Acknowledgement

We thank Anshika Maheshwari (HZI) for her excellent technical assistance with the quantification of compound uptake in the *E. coli* model and Dr. Raimo Franke (HZI) for fruitful discussions. Further, we want to thank Alexander Hipp and Jörg Hammel for processing the obtained X-ray microtomography data and improving the sample preparation. The tomographic investigations were performed within the DESY Beamtime Proposal ID I-2917023.

References

1. Peleg , A. Y., and Hooper , D. C. (2010) Hospital-acquired infections due to Gram-negative bacteria. *N. Engl. J. Med.* 362, 1804-1813. DOI:10.1056/NEJMra0904124.
2. Masi, M., Réfregiers, M., Pos, K. M., and Pagès, J.-M. (2017) Mechanisms of envelope permeability and antibiotic influx and efflux in Gram-negative bacteria. *Nat. Microbiol.* 2, 17001. DOI:10.1038/nmicrobiol.2017.1.
3. Tommasi, R., Brown, D. G., Walkup, G. K., Manchester, J. I., and Miller, A. A. (2015) ESKAPEing the labyrinth of antibacterial discovery. *Nat. Rev. Drug Discov.* 14, 529-542. DOI:10.1038/nrd4572.
4. Silhavy, T. J., Kahne, D., and Walker, S. (2010) The bacterial cell envelope. *Cold Spring Harb. Perspect Biol.* 2, a000414. DOI:10.1101/cshperspect.a000414.
5. Graef, F., Gordon, S., and Lehr, C.-M. (2016) Anti-infectives in drug delivery - overcoming the Gram-negative bacterial cell envelope. In *How to Overcome the Antibiotic Crisis: Facts, Challenges, Technologies and Future Perspectives* (Stadler, M., and Dersch, P., Eds.), 475-496, Springer International Publishing, Cham.
6. Lewis, K. (2012) Antibiotics: Recover the lost art of drug discovery. *Nature* 485, 439-440. DOI:10.1038/485439a.
7. Richter, M. F., Drown, B. S., Riley, A. P., Garcia, A., Shirai, T., Svec, R. L., and Hergenrother, P. J. (2017) Predictive compound accumulation rules yield a broad-spectrum antibiotic. *Nature* 545, 299-304. DOI:299. 10.1038/nature22308.
8. Reller, L. B., Weinstein, M., Jorgensen, J. H., and Ferraro, M. J. (2009) Antimicrobial susceptibility testing: A review of general principles and contemporary practices. *Clin. Infect. Dis.* 49, 1749-1755. DOI:10.1086/647952.

9. Cinquin, B., Maigre, L., Pinet, E., Chevalier, J., Stavenger, R. A., Mills, S., Réfrégiers, M., and Pagès, J.-M. (2015) Microspectrometric insights on the uptake of antibiotics at the single bacterial cell level. *Sci. Rep.* 5, 17968. DOI:10.1038/srep17968.
10. van Weerd, J., Karperien, M., and Jonkheijm, P. (2015) Supported lipid bilayers for the generation of dynamic cell–material interfaces. *Adv. Healthc. Mater.* 4, 2743-2779. DOI:10.1002/adhm.201500398.
11. Nestorovich, E. M., Danelon, C., Winterhalter, M., and Bezrukov, S. M. (2002) Designed to penetrate: Time-resolved interaction of single antibiotic molecules with bacterial pores. *Proc. Natl. Acad. Sci. U. S. A.* 99, 9789-9794. DOI:10.1073/pnas.152206799.
12. Pages, J.-M., James, C. E., and Winterhalter, M. (2008) The porin and the permeating antibiotic: a selective diffusion barrier in Gram-negative bacteria. *Nat. Rev. Micro.* 6, 893-903. DOI:10.1038/nrmicro1994.
13. Kuzmenko, A. I., Wu, H., and McCormack, F. X. (2006) Pulmonary collectins selectively permeabilize model bacterial membranes containing rough lipopolysaccharide. *Biochemistry* 45, 2679-2685. DOI:10.1021/bi0522652.
14. Clifton, L. A., Holt, S. A., Hughes, A. V., Daulton, E. L., Arunmanee, W., Heinrich, F., Khalid, S., Jefferies, D., Charlton, T. R., Webster, J. R. P., Kinane, C. J., and Lakey, J. H. (2015) An accurate in vitro model of the E. coli envelope. *Angew. Chem. Int. Ed. Engl.* 54, 11952-11955. DOI:10.1002/anie.201504287.
15. Graef, F., Vukosavljevic, B., Michel, J.-P., Wirth, M., Ries, O., De Rossi, C., Windbergs, M., Rosilio, V., Ducho, C., Gordon, S., and Lehr, C.-M. (2016) The bacterial cell envelope as delimiter of anti-infective bioavailability – An in vitro permeation model of the Gram-negative bacterial inner membrane. *J. Control. Release* 243, 214-224. DOI:10.1016/j.jconrel.2016.10.018.
16. Artursson, P., and Karlsson, J. (1991) Correlation between oral drug absorption in humans and apparent drug permeability coefficients in human intestinal epithelial (Caco-2) cells. *Biochem. Biophys. Res. Commun.* 175, 880-885. DOI:10.1016/0006-291X(91)91647-U.
17. Lugtenberg, E. J. J., and Peters, R. (1976) Distribution of lipids in cytoplasmic and outer membranes of Escherichia coli K12. *Biochim. Biophys. Acta* 441, 38-47. DOI:10.1016/0005-2760(76)90279-4.
18. Takrouri, K., Cooper, H. D., Spaulding, A., Zucchi, P., Koleva, B., Cleary, D. C., Tear, W., Beuning, P. J., Hirsch, E. B., and Aggen, J. B. (2016) Progress against Escherichia coli with the oxazolidinone class of antibacterials: Test case for a general approach to improving whole-cell Gram-negative activity. *ACS Infect. Dis.* 2, 405-426. DOI:10.1021/acsinfecdis.6b00003.
19. Hancock, R. E. W. (1997) The bacterial outer membrane as a drug barrier. *Trends Microbiol.* 5, 37-42. DOI:10.1016/S0966-842X(97)81773-8.
20. Eggert, U. S., Ruiz, N., Falcone, B. V., Branstrom, A. A., Goldman, R. C., Silhavy, T. J., and Kahne, D. (2001) Genetic basis for activity differences between vancomycin and glycolipid derivatives of vancomycin. *Science* 294, 361. DOI:10.1126/science.1063611.
21. Zgurskaya, H. I., López, C. A., and Gnanakaran, S. (2015) Permeability barrier of Gram-negative cell envelopes and approaches to bypass it. *ACS Infect. Dis.* 1, 512-522. DOI:10.1021/acsinfecdis.5b00097.
22. Gallagher, L. A., McKnight, S. L., Kuznetsova, M. S., Pesci, E. C., and Manoil, C. (2002) Functions required for extracellular quinolone signaling by Pseudomonas aeruginosa. *J. Bacteriol.* 184, 6472-6480. DOI:10.1128/JB.184.23.6472-6480.2002.
23. Lu, C., Maurer, C. K., Kirsch, B., Steinbach, A., and Hartmann, R. W. (2014) Overcoming the unexpected functional inversion of a PqsR antagonist in Pseudomonas aeruginosa: An in vivo potent antivirulence agent targeting pqs quorum sensing. *Angew. Chem. Int. Ed. Engl.* 53, 1109-1112. DOI:10.1002/anie.201307547.
24. Storz, M. P., Maurer, C. K., Zimmer, C., Wagner, N., Brengel, C., de Jong, J. C., Lucas, S., Müschen, M., Häussler, S., Steinbach, A., and Hartmann, R. W. (2012) Validation of PqsD as an anti-biofilm target in Pseudomonas aeruginosa by development of small-molecule inhibitors. *J. Am. Chem. Soc.* 134, 16143-16146. DOI:10.1021/ja3072397.

25. Storz, M. P., Allegretta, G., Kirsch, B., Empting, M., and Hartmann, R. W. (2014) From in vitro to in cellulo: structure-activity relationship of (2-nitrophenyl)methanol derivatives as inhibitors of PqsD in *Pseudomonas aeruginosa*. *Org. Biomol. Chem.* 12, 6094-6104. DOI:10.1039/C4OB00707G.
26. Delcour A. H. (2009) Outer Membrane Permeability and Antibiotic Resistance. *Biochim. Biophys. Acta.* 5, 808-816. DOI: 10.1016/j.bbapap.2008.11.005
27. Santos R. S., Figueiredo C., Azevedo N. F., Braeckmans K., De Smedt S. C. (2017) Nanomaterials and molecular transporters to overcome the bacterial envelope barrier: Towards advance delivery of antibiotics. *Adv. Drug Deliv. Rev.* 1-20. DOI: 10.1016/j.addr.2017.12.010.
28. Hancock R.E.W., Bell A. (1988) Antibiotic uptake into bacteria. *Eur. J. Clin. Microbiol. Infect. Dis.* 7, 713-720.
29. Nikaido H. (2003) Molecular Basis of Bacterial Outer Membrane Permeability Revisited. *Microbiol. Mol. Biol. Rev.* 67, 593-656. DOI: 10.1128/MMBR.67.4.593-656.2003
30. Mortimer P. G. S., Piddock L. J. V. (1993) The accumulation of five antibacterial agents in porin-deficient mutants of *Escherichia coli*. *J. Antimicrob. Chemother.* 32, 195-213.
31. Takács-Novák K., Józsan M., Hermecz I., Szász G. (1992) Lipophilicity of antibacterial fluoroquinolones. *Int. J. Pharm.* 79, 89-96. DOI: 10.1016/0378-5173(92)90099-N.
32. Chemicalize was used for ciprofloxacin, erythromycin, nalidixic acid, norfloxacin, novobiocin, pipemidic acid, rifampicin, tetracycline to predict LogD_{pH7.5} and for ciprofloxacin, norfloxacin, pipemidic acid and nalidixic acid to predict microspecies distribution, 03/2018, <https://chemicalize.com/> developed by ChemAxon (<http://www.chemaxon.com>)
33. Cramariuc O., Rog T., Javanainen M., Monticelli L., Polishchuk A. V., Vattulainen I. (2012) Mechanism for translocation of fluoroquinolones across lipid membranes. *Biochim. Biophys. Acta* 1818, 2563-2571. DOI: 10.1016/j.bbamem.2012.05.027.
34. Nikaido, H. (1988) Bacterial resistance to antibiotics as a function of outer membrane permeability. *J. Antimicrob. Chemother.* 22, 17-22.
35. Piddock, L. J. V., and R. Wise. 1986. The effect of altered porin expression in *Escherichia coli* upon susceptibility to 4 quinolones. *J. Antimicrob. Chemother.* 18, 547-549.
36. Bajaj. H., Gutierrez S. A., Bodrenko I., Mallocci G., Scorciapino M. A., Winterhalter M., Ceccarelli M. (2017) Bacterial Outer Membrane Porins as Electrostatic Nanosieves: Exploring Transport Rules of Small Polar Molecules. *ACS Nano* 11, 4598-4606. DOI: 10.1021/acsnano.6b08613.
37. O'Shea, R., and Moser, H. E. (2008) Physicochemical properties of antibacterial compounds: Implications for drug discovery. *J. Med. Chem.* 51, 2871-2878. DOI:10.1021/jm700967e.
38. Ishinaga, M., Kanamoto, R., and Kito, M. (1979) Distribution of phospholipid molecular species in outer and cytoplasmic membranes of *Escherichia coli*. *J. Biochem.* 86, 161-165.

For table of contents only

